35th Annual International Conference of the IEEE EMBS
Osaka, Japan, 3 - 7 July, 2013

Haptic fMRI : Combining Functional Neuroimaging with Haptics for Studying the Brain's Motor Control Representation

Samir Menon[1], Gerald Brantner[1], Chris Aholt[1], Kendrick Kay[2], and Oussama Khatib[1]

***Abstract*— A challenging problem in motor control neuroimaging studies is the inability to perform complex human motor tasks given the Magnetic Resonance Imaging (MRI) scanner's disruptive magnetic fields and confined workspace. In this paper, we propose a novel experimental platform that combines Functional MRI (fMRI) neuroimaging, haptic virtual simulation environments, and an fMRI-compatible haptic device for real-time haptic interaction across the scanner workspace (above torso ~ .65x.40x.20m^3). We implement this Haptic fMRI platform with a novel haptic device, the Haptic fMRI Interface (HFI), and demonstrate its suitability for motor neuroimaging studies. HFI has three degrees-of-freedom (DOF), uses electromagnetic motors to enable high-fidelity haptic rendering (>350Hz), integrates radio frequency (RF) shields to prevent electromagnetic interference with fMRI (temporal SNR >100), and is kinematically designed to minimize currents induced by the MRI scanner's magnetic field during motor displacement (<2cm). HFI possesses uniform inertial and force transmission properties across the workspace, and has low friction (.05–.30N). HFI's RF noise levels, in addition, are within a 3 Tesla fMRI scanner's baseline noise variation (~.85± .1%). Finally, HFI is haptically transparent and does not interfere with human motor tasks (tested for .4m reaches). By allowing fMRI experiments involving complex three-dimensional manipulation with haptic interaction, Haptic fMRI enables—for the first time—non-invasive neuroscience experiments involving interactive motor tasks, object manipulation, tactile perception, and visuo-motor integration.**

I. Introduction

Since its invention, fMRI has rapidly developed as a reliable, non-invasive, and high-resolution (mm, sec) neuroimaging technique [1], [2], but its application to motor control and rehabilitation experiments has been limited by an inability to precisely monitor and perturb motions or recreate motor tasks inside MRI scanners. Force-controlled haptic devices [3] and virtual simulations [4], [5], [6] have overcome these limitations outside MRI scanners, and have been actively used in rehabilitation [7], [8] and motor neuroscience [9]. Integrating such haptics with fMRI will allow us to overcome past research's limitations, which confined it to non-interactive free-space motions.

Combining haptics with fMRI for motor neuroscience studies, however, poses many challenges. The haptic device's kinematics must allow complex motions that span the scanner's bore. The device must also be haptically transparent and possess uniform inertial and force transmission properties across its workspace. The sensing, control, and simulation system must be accurate, support a sufficient control frequency to simulate motor tasks [3], and allow high-fidelity haptic simulations in virtual worlds. Finally, and most importantly, the haptic device must be *fMRI-compatible*—it must reliably operate in the scanner's high magnetic fields without introducing RF noise.

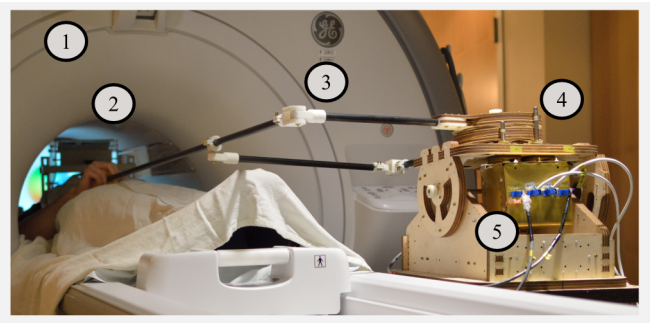

Fig. 1. Haptic fMRI. (*1*) Our novel three DOF fMRI-compatible haptic device, HFI, operating in a 3T MRI scanner. The subject uses mirrors to view a haptic simulation (*2*, painting) and interacts with it by manipulating HFI's four-bar linkage (*3*). Cable actuation (*4*) and RF shields (*5*) help minimize RF noise.

Past research on developing fMRI-compatible haptics for motor control experiments has produced numerous mechanical design, control, and actuation strategies. Since electromagnetic actuation complicates fMRI compatibility, much work has focused on elecro-active polymer [10], pneumatic [11], and hydraulic [12], [13] actuators. Recent research [14] has also studied the dynamic effects of cables connecting a remote actuator to an articulated joint in the MRI machine. An alternative approach used a shielded PHANTOM [15], [16] device connected to a long carbon fiber rod that was attached to a linear rail at its midpoint, which constrained the workspace. An unresolved challenge facing all such approaches, however, is to achieve high-fidelity force control, natural motions [17] and uniform inertial properties across a large three-dimensional workspace.

This paper outlines a Haptic fMRI system built using the HFI, a three DOF, magnet-safe haptic device that spans the entire MRI scanner workspace (Fig. 1). First, we present a novel design that uses shielded electromagnetic actuators, and minimizes motor motion (<2cm), to enable high-fidelity fMRI-compatible haptics. Second, we demonstrate that HFI's inertial and force transmission properties are uniform across the workspace—the condition numbers vary by 1.3%, and

*This work was supported by BioX, Stanford University

[1]S. Menon, G. Brantner, C. Aholt, and O. Khatib are with the Artificial Intelligence Laboratory, Department of Computer Science, Stanford University, Stanford, CA 94305, USA smenon@stanford.edu, geraldb@stanford.edu, cjaholt@stanford.edu, ok@cs.stanford.edu

[2]K. Kay is with the Department of Psychology, Stanford University, Stanford, CA 94305, USA knk@stanford.edu

978-1-4577-0216-7/13/$26.00 ©2013 IEEE

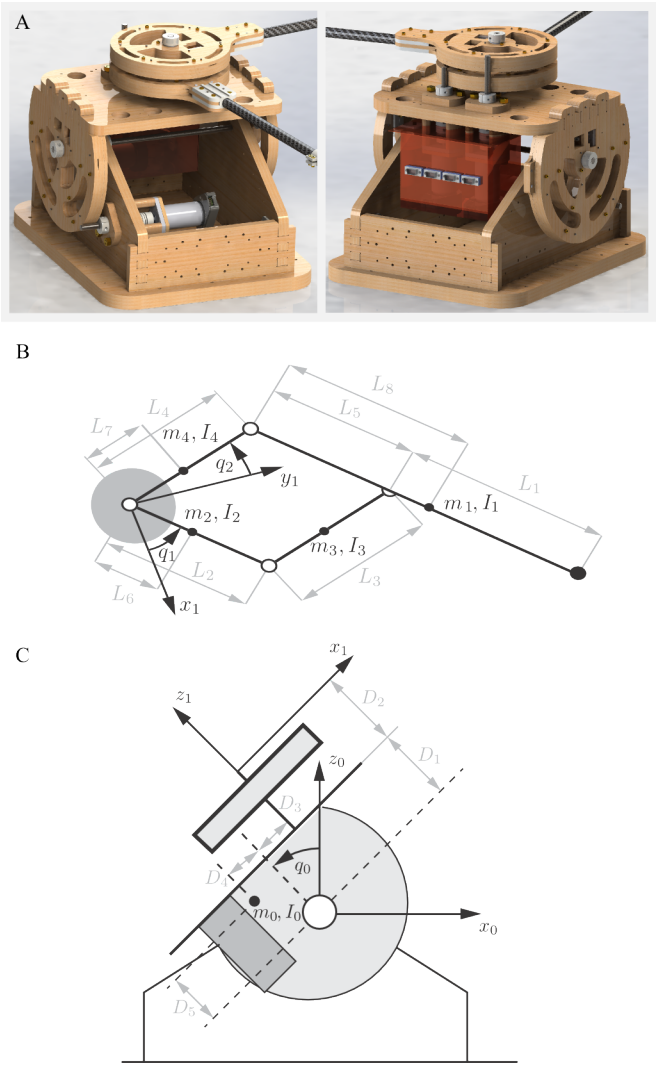

Fig. 2. Device Design. (*A*) The motors are bolted to the structure and encased in a Brass Faraday cage with capacitive filters at electrical junctions. (*B, C*) HFI's kinematics allow remote motor placement and a large workspace. The three DOF are q_2 and q_1 (*B*), and q_0 (*C*). Kinematic variables shown can be tuned to optimize inertial and force properties.

3.7%, respectively. Third, we show that HFI can reliably monitor trial-to-trial motion variability during interactive three-dimensional haptic simulations in a 3 Tesla MRI scanner. Fourth, we demonstrate that HFI's RF noise interference is below trial-to-trial variability in fMRI scans while imaging a human subject, which ensures its compatibility with fMRI experiments. Finally, we demonstrate that HFI does not affect human manipulation trajectories for motions larger than the MRI workspace can support, obviating any device-related experimental confounds.

II. HFI's Design and Performance

A. fMRI-Compatible Design

Our primary goal while developing HFI was to enable neuromuscular control experiments that combine neuroimaging with haptic interaction in immersive virtual worlds [4], [18]. Our first constraint was high-fidelity haptic interaction, for which we chose electromagnetic motors that provide a control rate beyond human perception of motion direction and static forces (0.4-100Hz [3]). We selected motors with the minimum possible inertia, which could allow emulating the weight of common objects (0-250g, 0-2.5N). Our next constraint was avoiding magnet-motor attraction, which required using a large four-bar linkage to place motors beyond the 200 Gauss line (>1m from the bore). Finally, we minimized magnetic induction currents due to motor displacement.

We developed a gravity-balanced design that rigidly attaches the electromagnetic motors (Maxon RE40 148877 brushed DC) and encoders (US Digital E6-2500) to a stable structure (Fig. 2A). Minimizing motor displacement is necessary to minimize eddy currents induced by the MRI scanner's magnetic field gradients. HFI's z-axis motor is stationary and attached to the base. The x-y-axis motors are both attached to a rigid upper plate, and are positioned to gravity-balance the four-bar linkage at the center of the workspace. Since the z-axis workspace is small and the linkage has a long arm (1.3m), the x-y-axis motor movements are minimized (~2cm).

The next step was to design a backlash-free force transmission to the four-bar linkage that maintains the noise shielding. Doing so required avoiding metallic contacts that could cross the shield boundary and act as RF antennas. As such, we connected the shafts to custom-made plastic shaft-couplers (laser-sintered polyamide), and the coupler to non-magnetic Titanium shafts such that the coupler spanned the shield boundary (Fig. 2A). Next, we connected the extruded motor shafts to wooden capstans using Kevlar® cables. To minimize friction and backlash, we selected the minimal diameter cable (DuPont; mil spec A-A-55220; .29mm diameter) that reliably sustained HFI's operating forces. We built the four-bar parallelogram linkage with non-magnetic carbon fiber, brass screws and bolts, ceramic bearings, and plastic joints, which are all fMRI-compatible. Using carbon fiber tubes (.625" dia, .055" thickness) maximized the structural stiffness while maintaining low weight and inertia.

After developing the shields, transmission, and linkage, our tests indicated that the primary noise source was not the mechanical operation of HFI, but the control electronics. Placing the electronics outside the scan room, however, was not enough since the connecting wires acted as antennas. To minimize RF interference in fMRI's 20-150 MHz range [19], we placed capacitive filters (820pf, L-com DGFC9MF) at the Faraday cage enclosing the scan room, as well as at the Faraday cage enclosing the motors. Passing all the motor and encoder wiring through the filters reduced the RF noise to imperceptible levels (Fig. 5C).

B. HFI Achieves Haptic Transparency With Uniform Inertias and Forces, and Low Friction

Haptic transparency measures the resistance a device provides when a user applies forces to move it. We characterized HFI's transparency by computing its effective inertia, which must be uniform to prevent subjects from perceiving mass changes during motion, and its force properties, which lie

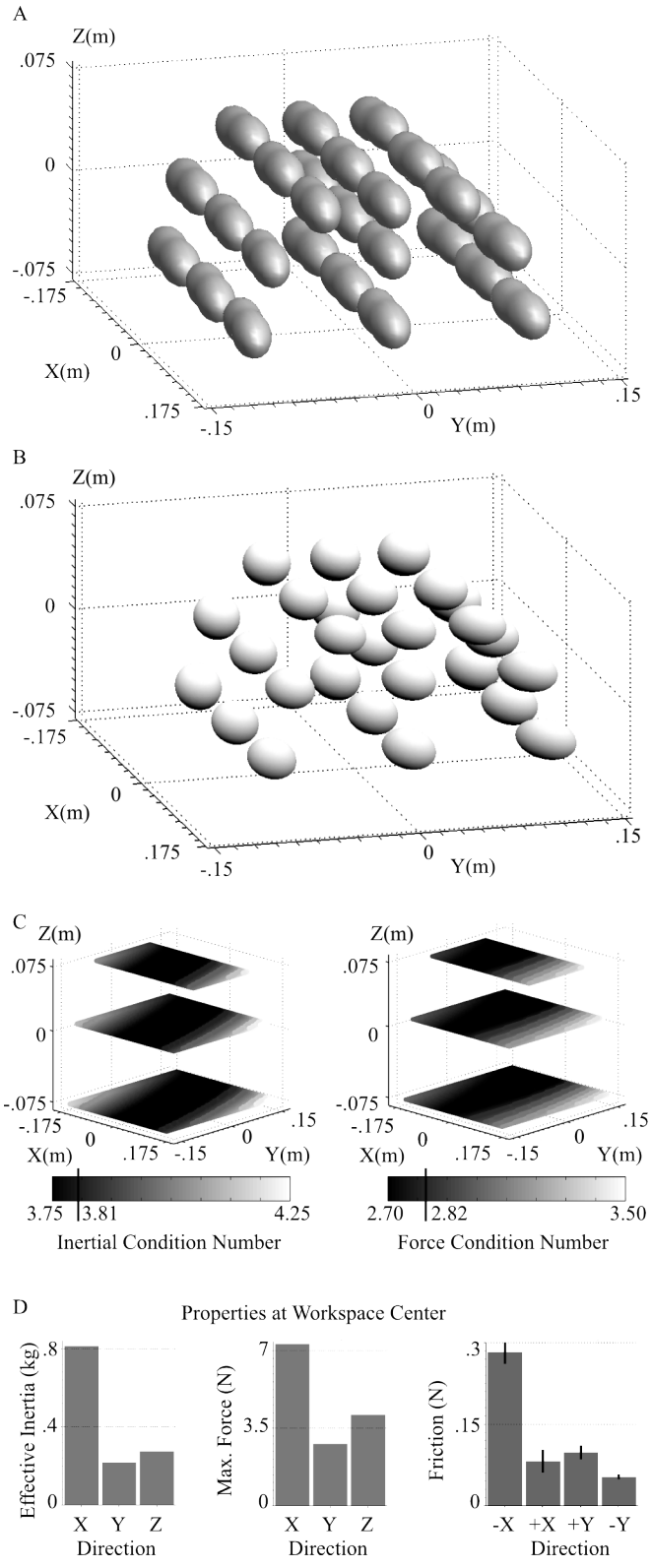

Fig. 3. Device Characteristics. (*A*) HFI's inertial properties projected to the end-effector (belted ellipsoids) are similar across the scanner workspace. (*B*) The force transmission properties, like the inertias, are uniform across the workspace. (*C*) The condition numbers in the three planes for both the inertial and force properties demonstrate their uniformity (means marked on colorbar). (*D*) Effective inertia, maximum force, and friction properties at the workspace center. Friction plots indicate the bootstrap mean and 95% C.I. (12 samples/direction).

between the supremum of the friction and infimum of the transmitted forces. We determined HFI's inertial and force properties by physically measuring material densities, using our CAD model to compute each rigid link's inertias, and then creating a detailed articulated body model (Fig. 2). The end-effector inertial properties [20] are the locus of a vector x given by:

$$x^T \left(J_{hand}\, A^{-1}\, J_{hand}^T\right) x / \sqrt{x^T\, x} = 1, \tag{1}$$

where J_{hand} is the translation Jacobian at the grasp point and A is the generalized inertia matrix. We computed A using the articulated body structure and the motor inertias:

$$A = A_{trans.} + A_{rot.} + A_{motor} \tag{2}$$

$$A_{trans.} = \sum_{i=0}^{4} m_i\, J_{com_i}^T\, J_{com_i} \tag{3}$$

$$A_{rot.} = \sum_{i=0}^{4} J_{\omega\, com_i}^T\, I_{com_i}\, J_{\omega\, com_i} \tag{4}$$

$$A_{motor} = \sum_{i=0}^{2} I_{motor_i}. \tag{5}$$

The force transmission is the locus of Euclidean end-effector forces produced by unit generalized forces (motor torques).

We plotted the inertial *belted ellipsoids* at a set of grasp points spanning the MRI workspace (Fig. 3A). HFI's end-effector inertial properties are uniform (Fig. 3C) across the workspace, which is necessary for neuroscience experiments where changing inertias might require changing the neural control signals. The inertia matrix mean condition number across the workspace was 3.810, bootstrap 95% C.I. 3.807–3.120. The uniform inertial properties are because we designed HFI to operate in a narrow joint angle range ($q_0 \epsilon$ [-7.77, 6.83] , $q_1 \epsilon$ [-5.20, 14.82] , $q_2 \epsilon$ [-44.44, 42.15] degrees) within the scanner, avoiding kinematic singularities.

As with the inertial ellipsoids, we plotted the force transmission characteristics across the MRI workspace (Fig. 3B) and found them to be uniform (Fig. 3C). The Jacobian mean condition number across the workspace was 2.826, bootstrap 95% C.I. 2.821–2.830. We also computed the maximum forces at the center of the workspace using a line search along x, y, and z, computed required torques using the Jacobian, and stopped when a maximum joint torque was exceeded. The plots demonstrate that HFI's force levels exceed our requirement of 2.5N across the workspace.

Measuring friction in robots [21] is complicated because of two reasons. First, measuring friction requires gravity compensation, but both motor torques and friction stabilize HFI and delineating their contribution is hard for its low friction levels. Second, friction properties change with a variety of factors such as humidity, temperature, duration of operation, and the cable drive's tension. We did, however, estimate sliding friction (sensor noise +/-.025N; readings rounded to .05N) at the center of the workspace where HFI is gravity balanced by design, and found anisotropic but small fiction forces (Fig. 3D (right)).

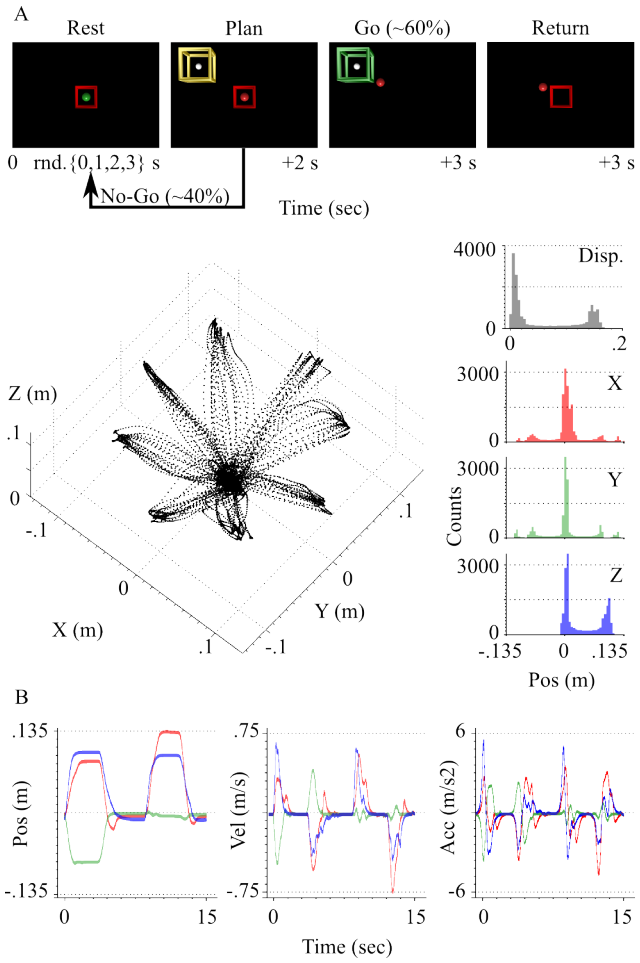

Fig. 4. Device performance in the MRI scanner. (*A*). Visually guided reach trajectories monitored with HFI for two fMRI scan runs (265sec each, subject S2). The horizontal axis represents time, the rest duration is randomized, and the plan is followed by either a go cue (60%) or a no-go cue (40%). The red ball represents the controlled haptic point, and it turns green when the desired position is reached. The white ball is the desired point. The cage provides depth perception. Histograms demonstrate the trajectory's overall displacement (black), x motion (red), y motion (green), and z motion (blue). (*B*). The end-effector position, velocity, and acceleration for two reaches.

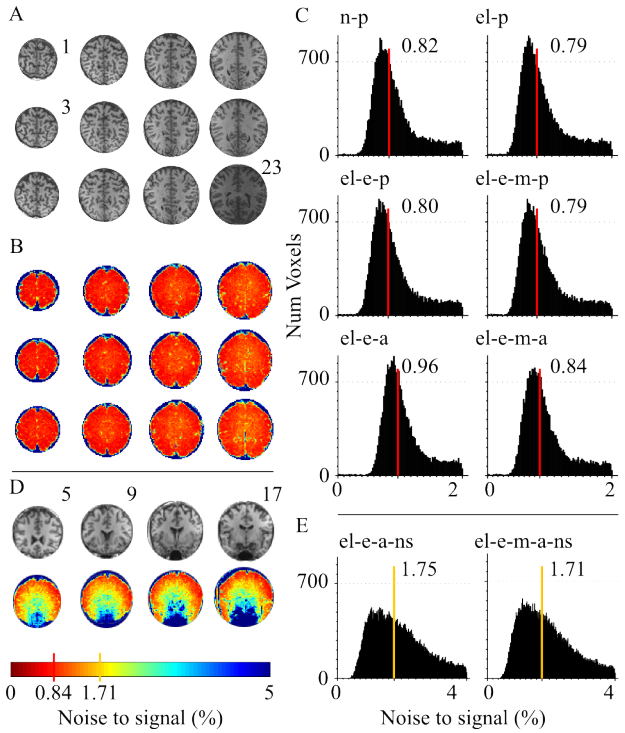

Fig. 5. RF noise testing in the MRI scanner. (*A*). Brain slices imaged with fMRI span motor and visual cortex for subject S2. 24 slices were angled at ~45 degrees to the transverse ear-nose plane and grow in diameter moving inwards from the skull to the brain's center (odd slices, 1–23, shown for clarity). (*B*). Temporal signal to noise heatmap with subject operating HFI while electronics, encoders and motors are engaged. (*C*). Histogram of voxel noise-to-signal ratios for nothing (n), electronics (el), encoders (e), and/or motors (m) engaged, while the subject was passive (p, device moved by fMRI operator) or active (a). The motor task was painting on virtual paper (see Fig. 1). Red bar and numeric value indicate the bootstrap noise median (95% C.I $<$ .01 for all). (*D, E*). Noise without shields (ns) is much higher (slices 5, 9, 13, 17 shown for clarity). Note different histogram scales.

C. HFI Enables Interactive Motor Tasks in MRI Scanners

To characterize HFI's performance inside the MRI scanner, we created a three-directional reaching experiment where subjects would be shown a visual cue and would move a virtual ball to the cue position (Fig. 4). Subjects executed closed-loop (with visual feedback) reaches to a randomly selected direction out of eight evenly distributed directions on a circle, in a plane above their chest. Subjects were first given a random duration rest, then shown a goal cue to plan the motion, then either a rest cue again or a go cue to move to the position (Fig. 4A). The randomized *go* vs. *no-go* paradigm made sure the subjects were attentive.

HFI's high encoder counts helped accurately monitor trajectories (position err $<$.025mm). Subjects exhibited large variability across motions, and the three modes of the movement histograms (Fig. 4A (right)) also demonstrate that subjects could not precisely maintain the goal positions. Such unobserved variability can reduce the statistical power of neuroscience experiments. Our results thus reiterate the need for using haptics to monitor subjects during fMRI motor experiments.

III. HFI's RF Noise Characteristics

To characterize HFI's RF noise interference with fMRI scans in a real-world setting, we scanned a human subject's motor and visual cortices for six conditions (Fig. 5): *(n-p)* Powered down device and passive subject (did not move); *(el-p)* control electronics on and passive subject; *(el-e-p)* encoders were on, motors were off, and operator moved HFI; *(el-e-m-p)* encoders were on, motors were on, and operator moved HFI; *(el-e-a)* encoders were on, motors were off, and subject moved HFI; and *(el-e-m-a)* encoders were on, motors were on, and subject moved HFI. The *(ns)* conditions were without shielding. These scan conditions exhaustively test RF noise from the electronics, encoders, and motors, as well as control for subject head motion covariates (noise increases in *a* vs. *p*).

For each scan condition, we computed the temporal signal-to-noise ratio (tSNR) [22] using the noise median around the blood oxygenation level dependent (BOLD) signal. We did

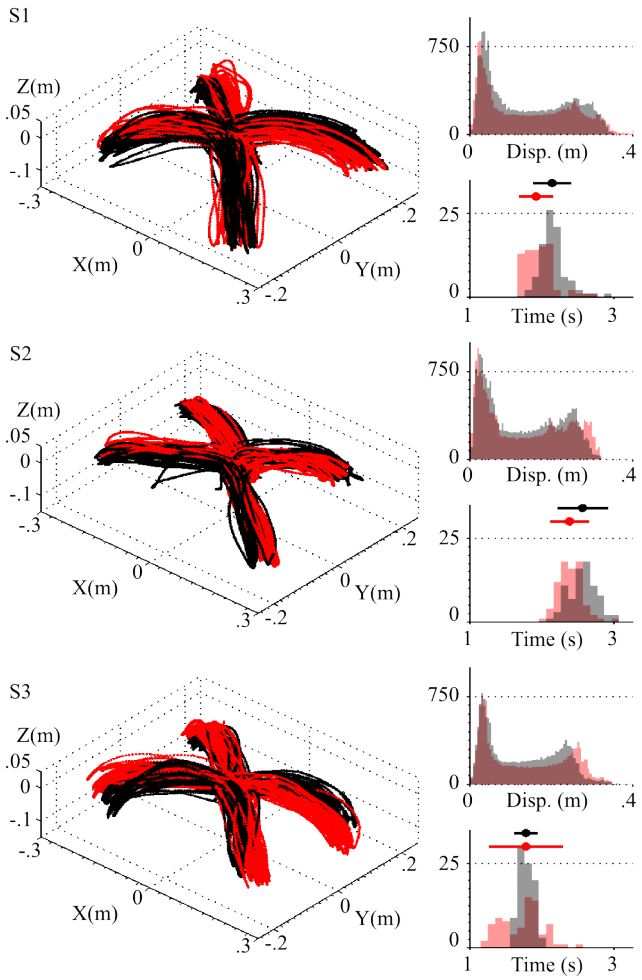

Fig. 6. Haptic Transparency. Three-dimensional reaches in four directions observed using optical motion capture for two conditions: holding either nothing (red, 20/direction) or HFI (black, 20/direction). The three subjects' (*S1*, *S2*, *S3*) motions were similar with and without HFI. The trajectories (left), hand-displacement histograms (right-above, 100Hz samples), and reach-timing histograms (right-below, 20x4=80/condition) are shown for all three subjects. Error bars on trial-times indicate bootstrap median 95% C.I.

so by regressing out a line from each voxels time-series, computing the absolute value of the difference between successive time points, computing the median of these absolute differences, dividing the result by the mean of the original time-series, and then multiplying by 100. The noise levels while the subject operated HFI with electronics, motors, and encoders (Fig. 5B) were predominantly below 1% and were similar to all other conditions (Fig. 5C). We noted that re-shimming the scanner before each scan run substantially improved the tSNR by preventing magnetic field drift.

Our RF noise characterization tests demonstrate that HFI operates with insignificant noise not only at the cortical surface, but also within deeper brain regions like white matter (Fig. 5B). Moreover, our tests demonstrate that electromagnetic motors are a viable actuation mechanism within MRI machines if they are remotely situated, shielded, fixed to a rigid body, and have filtered electrical connections.

IV. Haptic Transparency Tests With Humans

To verify that our uniform inertias and low friction produced haptic transparency, we experimentally tested HFI's influence on human motions. We did so by comparing free-space unguided reaching motions (larger than scanner workspace) for three subjects, with and without holding HFI (Fig. 6). Each subject performed 20 reaches from above their solar-plexus to their shoulders and the corners of their waist. We monitored these motions using an optical motion capture system (see Appendix for details). For free and haptic motions, we compared reaching trajectories, displacement histograms, and trial-time histograms. The reach trajectories and displacement histograms overlapped, were bimodal, and indicated that two subjects made slightly shorter reaches while holding HFI. Finally, the time taken to execute the reaches was unimodal but the median distribution overlapped (bootstrap 95% C.I.).

V. Conclusions and Discussion

In this paper, we present—to our knowledge—the first three DOF force-controlled and electromagnetically-actuated haptic device that can conduct motor control experiments across the entire MRI scanner workspace. HFI can accurately monitor a subject's hand position, velocity, and acceleration, and can apply forces with a sufficient control rate to perturb motions and enable virtual manipulation tasks. It operates without RF interference in the scanner room while scanning at a higher fMRI spatial resolution than past devices (~2x of [11] and [15]). Finally, combined with the CHAI3D [18] haptics rendering platform, HFI can replicate a variety of manipulation tasks in immersive virtual simulations. Stepping beyond past experiments with unguided and unmonitored joint motions [2], and limited [12], [13] or planar [11] hand movements, HFI promises to reveal novel insights into human motor coordination and control.

Our mechanical design, shielding, and scanning protocols overcome RF interference challenges faced by past research [12]. We attribute our results to numerous unique factors including limited motor motion, a solid brass grounded Faraday cage, control electronics outside the MRI room, capacitive filters at electrical junctions, shimming before each run, and fieldmaps to correct magnetic field drift. The GE MR750 scanner's shimming advances, and 32-channel head-coil's large signals, also increase SNR [19].

Since numerous factors influence any MRI-compatible haptic device's performance and noise characteristics, a set of quantifiable *Haptic fMRI* metrics are important to summarize device performance. We outline some metrics that summarize noise and other experimental confounds (Table. I), and look forward to improving HFI's performance as well as the metrics themselves. Head motion, in particular, induces task-correlated noise that is hard to remove from fMRI signals, and characterizing its effect on Haptic fMRI experiments is an immediate goal.

TABLE I
HAPTIC DEVICE METRICS

Metric	Desired	HFI
Position error	$<$1 *mm* [3], [5]	~.025 *mm*
End-effector force	~2.5 *N*	7.8, 2.8, 4.1 *N (x,y,z)*
End-effector inertia	minimal	.81, .22, .27 *kg (x,y,z)*
End-effector friction	minimal	.05–.40 *N*
Inertia condition no.	1	3.81
Force condition no.	1	2.82
Control update rate	0-100 *Hz* [3]	$>$350 *Hz*
Workspace	~.65x.40x.20 m^3	$>$.75x1.00x.75 m^3
Peak Head Motion	minimal	$<$.1 *mm*
Total Head Motion	minimal	$<$1 *mm*
Temporal Noise	$>$50 [22]	$>$100

APPENDIX

fMRI Scanning: All fMRI scans were conducted at Stanford University's Center for Cognitive and Neurobiological Imaging on a GE Discovery MR750 3 Tesla MRI scanner, with a 32 channel Nova Medical head coil. The scan protocol was gradient echo EPI with a 16cm field of view sampled at a 64x64 resolution (2.5x2.5x2.5 mm^3 voxels), a 1.57s repetition time, a 28ms echo time, and a 72^o flip angle. All scan runs were preceeded by 2^{nd}-order polynomial shimming and were sandwiched by fieldmap scans. After scanning, the fMRI images were slice time corrected, motion corrected (SPM), spatially undistorted using fieldmaps, and analyzed to compute temporal signal-to-noise. A subject-customized bite-bar minimized head motion. All runs (265 sec each) had frame-to-frame head motion $>$0.1mm or overall head motion $>$1mm.

Haptic Data: Motions were right handed. The haptic control loop was ~350Hz. For post-processing, haptic trajectories were filtered with a low-pass 25Hz zero-phase forward and reverse digital IIR filter using Matlab to remove high frequency noise. Trajectories were down-sampled to 100Hz using a cubic spline to simplify figure plotting.

Human Subjects: Subjects were healthy right-handed males with no history of motor disorders: S1, 28yr, 185lb, 5'9"; S2, 29yr, 165lb, 5'8"; S3, 20yr, 160lb, 5'8". Informed consent was obtained in advance on a protocol approved by the Institutional Review Board (IRB) at Stanford University.

Motion Capture: Motions were right handed. A Vicon Blade optical marker tracking system captured natural-motion and haptic-use trajectories. One marker was placed on each subject's middle knuckle, and was monitored at 120Hz. Trajectories were down-sampled to 100Hz using a cubic spline to simplify figure plotting.

ACKNOWLEDGMENTS

We gratefully acknowledge Francois Conti's assistance in designing and building HFI. We also thank Reuben Brewer and Prof. Kenneth Salisbury for advising us how to design and rapidly prototype haptic devices. Finally, we thank Laima Baltusis and Robert Dougherty for helping develop fMRI scanning and data processing protocols.

REFERENCES

[1] N. K. Logothetis, "What we can do and what we cannot do with fmri," *Nature*, vol. 453, no. 7197, pp. 869–878, Jun 2008.
[2] J. D. Meier, T. N. Aflalo, S. Kastner, and M. S. A. Graziano, "Complex organization of human primary motor cortex: A high-resolution fMRI study," *Journal of Neurophysiology*, vol. 100, pp. 1800–1812, 2008.
[3] K. Hale and K. Stanney, "Deriving haptic design guidelines from human physiological, psychophysical, and neurological foundations," *Computer Graphics and Applications, IEEE*, vol. 24, no. 2, pp. 33 –39, March-April 2004.
[4] J. K. Salisbury, F. Conti, and F. Barbagli, "Haptic rendering: Introductory concepts," *IEEE Computer Graphics and Applications*, vol. 24, no. 2, pp. 24–32, March 2004.
[5] F. Conti and O. Khatib, "Spanning large workspaces using small haptic devices," *Proc. of the Eurohaptics on Haptic Interfaces for Virtual Environment and Teleoperator Systems*, pp. 183–188, Mar. 2005.
[6] ——, "A new actuation approach for haptic interface design," *The International Journal of Robotics Research*, vol. 28, no. 6, pp. 834–848, 2009.
[7] H. Sveistrup, "Motor rehabilitation using virtual reality," *Journal of NeuroEngineering and Rehabilitation*, vol. 1, no. 1, p. 10, 2004.
[8] J. Broeren, M. Rydmark, A. Bjrkdahl, and K. S. Sunnerhagen, "Assessment and training in a 3-dimensional virtual environment with haptics: A report on 5 cases of motor rehabilitation in the chronic stage after stroke," *Neurorehabilitation and Neural Repair*, vol. 21, no. 2, pp. 180–189, March-April 2007.
[9] R. Shadmehr, M. A. Smith, and J. W. Krakauer, "Error correction, sensory prediction, and adaptation in motor control," *Annual Review of Neuroscience*, vol. 33, no. 1, pp. 89–108, 2010.
[10] J. Vogan, A. Wingert, J. Plante, S. Dubowsky, M. Hafez, and D. Kacher, "Manipulation in mri devices using electrostrictive polymer actuators: with an application to reconfigurable imaging coils," in *IEEE International Conference on Robotics and Automation*, 2004, pp. 2498–2504.
[11] J. Diedrichsen, Y. Hashambhoy, T. Rane, and R. Shadmehr, "Neural correlates of reach errors," *The Journal of Neuroscience*, vol. 25, no. 43, pp. 9919–9931, 2005.
[12] E. Burdet, R. Gassert, G. Gowrishankar, and H. Bleuler, "fmri compatible haptic interfaces to investigate human motor control," *Experimental Robotics IX*, vol. 21, pp. 25–34, 2006.
[13] S. Klare, A. Peer, and M. Buss, "Development of a 3 dof mr-compatible haptic interface for pointing and reaching movements," *Lecture Notes in Computer Science*, vol. 6192, pp. 211–218, 2010.
[14] D. Chapuis, R. Gassert, G. Gowrishankar, E. Burdet, and H. Bleuler, "Investigation of a cable transmission for the actuation of mr compatible haptic interfaces," in *Proc. of Biomedical Robotics and Biomechatronics*, 2006, pp. 426–431.
[15] A. Hribar, B. Koritnik, and M. Munih, "Phantom haptic device upgrade for use in fmri," *Medical and Biological Engineering and Computing*, vol. 47, pp. 677–684, 2009.
[16] T. Massie and J. Salisbury, "The phantom haptic interface: A device for probing virtual objects," in *Proceedings of the ASME winter annual meeting, symposium on haptic interfaces for virtual environment and teleoperator systems*, vol. 55, no. 1. IOS Press, 1994, pp. 295–300.
[17] M. Kostic, D. Popovic, and M. Popovic, "Influence of planar manipulandum to the hand trajectory during point to point movement," in *IEEE International Conference on Rehabilitation Robotics*, July 2011, pp. 1–4.
[18] F. Conti, F. Barbagli, D. Morris, and C. Sewell, "CHAI 3D — An open-source library for the rapid development of haptic scenes," in *Proc. of the Eurohaptics on Haptic Interfaces for Virtual Environment and Teleoperator Systems*, Pisa, Italy, March 2005.
[19] B. L. Schmitz, A. J. Aschoff, M. H. Hoffmann, and G. Grn, "Advantages and pitfalls in 3t mr brain imaging: A pictorial review," *American Journal of Neuroradiology*, vol. 26, no. 9, pp. 2229–2237, 2005.
[20] O. Khatib, "Inertial properties in robotic manipulation: An object-level framework," *International Journal of Robotics Research*, vol. 14, no. 1, pp. 19–36, 1995.
[21] C. Richard, M. R. Cutkosky, and K. MacLean, "Friction identification for haptic display," in *Proc. of the 1999 ASME IMECE*, Nov 1999.
[22] K. Murphy, J. Bodurka, and P. A. Bandettini, "How long to scan? the relationship between fmri temporal signal to noise ratio and necessary scan duration," *NeuroImage*, vol. 34, no. 2, pp. 565 – 574, 2007.